Int J Clin Exp Med 2017;10(8):11442-11453
www.ijcem.com /ISSN:1940-5901/IJCEM0053708

Original Article

Gadopentetic acid-doped, multifunctional, potentially targeted mesoporous silica nanoparticles as a novel MRI nano-contrast agent: synthesis, characterization and MRI study

Xue Zhou[1], Wei Jiang[1], Jiuling Zheng[2], Jiannong Zhao[1], Wei Wu[1], Dajing Guo[1], Xinjie Liu[1], Haitao Ran[3], Xiaojing He[1]

Departments of [1]Radiology, [2]Hepatobiliary, The Second Affiliated Hospital of Chongqing Medical University, No. 74 Linjiang Rd, Yuzhong District, Chongqing 400010, China; [3]Institute of Ultrasound Imaging, Department of Ultrasound, The Second Affiliated Hospital of Chongqing Medical University, No. 74 Linjiang Rd, Yuzhong District, Chongqing 400010, China

Received March 24, 2017; Accepted July 2, 2017; Epub August 15, 2017; Published August 30, 2017

Abstract: Gadolinium-doped mesoporous silica nanoparticles (Gd-MSNs) with potential molecular targeting capability have drawn worldwide attention as a magnetic resonance imaging (MRI) contrast agent. However, to date, Gd-MSNs have exhibited less-than-ideal properties. In this study, a reverse microemulsion method was used to dope gadopentetic acid (GA) into the mesopores of mesoporous silica nanoparticles (MSNs) to synthesize, for the first time, novel Gd-MSNs with high gadolinium content (GC). These Gd-MSNs were characterized using transmission electron microscopy (TEM) and a Malvern Zetasizer. The GCs and stability of the Gd-MSNs were determined by inductively coupled plasma-atomic emission spectroscopy (ICP-AES). Cell viability was tested via the Cell Counting Kit-8 (CCK-8) assay. Finally, cellular and rat MRI was performed to determine the *in vitro* and *in vivo* MR enhancing effects of the Gd-MSNs. We observed a clearly visible pore structure with a large number of doped GA molecules on the Gd-MSNs. The globular Gd-MSNs had higher GC and good stability in a simulated *in vitro* environment. No significant cellular toxicity was observed in either human umbilical vein endothelial cell (HUVEC) or human prostate adenocarcinoma cell (PC-3) lines at Gd-MSN concentrations of 25, 50, and 100 μg/mL. According to the cellular and rat MRI data, Gd-MSNs had strong MR enhancing effects both *in vitro* and *in vivo*. Gd-MSN is a promising novel MRI contrast agent for its multifunctional and highly efficient properties.

Keywords: Mesoporous silica nanoparticles, gadopentetic acid, nano-contrast agent, magnetic resonance imaging, reverse microemulsion

Introduction

Magnetic resonance imaging (MRI) is one of the most powerful techniques for clinical diagnoses [1], especially for the early diagnosis of tumors, because of its high soft tissue resolution [2, 3]. The application of MR contrast agents has further improved the diagnostic rate of tumors. Currently, MR contrast agents are mainly small-molecular gadolinium (Gd) chelates that are difficult to combine with biological macromolecules [4]. Thus, these contrast agents do not meet the requirements of modern theranostics, which requires contrast agents with good targeting ability to achieve molecular diagnosis and treatment [5]. Therefore, a novel carrier that can combine MR contrast agents and targeting groups is needed, and many researchers have recently conducted studies in this field [6-8].

Commonly used carriers include carbon nanotubes [9], superparamagnetic iron oxide nanoparticles (SPIONs) [10], liposomes and mesoporous silica nanoparticles (MSNs) [11]. All these nanoparticles (NPs) have several advantages over conventional imaging agents [12]. Loadability is one advantage, wherein the concentration of the imaging agent can be controlled within each NP during the synthesis process. Another advantage is the tunability of the surface of the NPs, which can potentially prolong

the circulation time of the agent in the blood or target a specific location within the body [13]. Of course, NPs also have some of their own characteristics. SPIONs are widely used as negative imaging agents, which produce a signal-decreasing effect [14]. Carbon nanotubes are both excellent contrast agents and efficient drug carriers, and they can be designed as positive or negative imaging agents, or both. However, carbon nanotubes are not hydrophilic and easily agglomerate in aqueous solutions, resulting in biological toxicity [15]. Liposomes can solve this problem because of their biocompatibility and are thought to have no toxic or injurious effects on biological systems [16]. However, the lipid composition of liposomes influences the relaxivity produced by the contrast agents encapsulated or incorporated within them. Compared with other NPs, MSNs possess larger surface areas and pore volumes; thus, they can be doped with larger amounts of contrast agent [17]. In addition, these NPs can be combined with antibodies, siRNA, aptamers or peptides for MR-targeted molecular diagnosis and treatment because of the rich abundance of easily modifiable hydroxyl groups on their surfaces [18-21]. Additionally, they can increase the sensitivity and specificity and decrease the dosage and toxic side effects of MR contrast agents [17].

MR contrast agents synthesized with MSNs as a carrier include magnetic iron oxide NPs, manganese (Mn), Gd, and others. Kim J et al. found that core-shell NPs consisted of a single Fe_3O_4 nanocrystal core and a dye-doped mesoporous silica shell with a poly (ethylene glycol) coating; these NPs can be used as MRI and fluorescence imaging agents and as drug delivery vehicles [22]. Kim T et al. synthesized mesoporous silica-coated hollow Mn oxide NPs as positive T_1 contrast agents for labeling and MRI tracking of adipose-derived mesenchymal stem cells [23]. Gd-based contrast agents are the most widely used due to their higher r_1 relaxation rate. Hsiao et al. found that Gadopentetate dimeglumine (Gd-DTPA) -modified MSNs were ideal T_1 contrast agents for tracking stem cells in MRI [24]. Shao et al. incorporated Gd_2O_3 molecules into the MSNs of Mobil Composition of Matter No. 41 (MCM-41) to obtain Gd_2O_3@MCM41 and demonstrated that this was superior to current contrast agents and could be used for tumor imaging in preclinical studies [25].

Many previous studies have used the classical Stöber method to synthesize Gd-containing MSNs [26-28]. However, NPs synthesized by this method usually have less-than-ideal properties, such as large particle sizes (> 100 nm), low gadolinium content (GC) (< 10%), irregular sphericity and poor dispersity [29, 30]. These properties may be caused by adding the Gd complex after synthesizing the MSNs, which could lead to the Gd complex attaching only to the NP surface. Thus, the attachment of the complex to the surface would decrease the regularity of both the dispersity and morphology of the NPs. Moreover, the preparation process of Gd-MSNs in many previous studies was divided into several complex steps to combine the Gd and NPs with poor reproducibility. To overcome these shortcomings, in this study, we improved the reverse microemulsion method [31] to simplify the preparation process and optimize the Gd-MSNs properties.

Reverse microemulsion can produce hydrophilic and fairly uniform-sized NPs and allows easy modulation of the NP surfaces for various applications [32-34]. This method had long been applied in the preparation of silica NPs but rarely been used during the synthesis of Gd-MSNs. In this study, we innovatively introduced gadopentetic acid (GA) solution into the microemulsion reaction system when synthesizing MSNs. GA was doped into Si-O-Si cages that were created by hydrolyzing tetraethylorthosilicate (TEOS) into the MSNs through this method. Thus, GA is one component of this reverse microemulsion reaction system. As a result, the amount of gadolinium loaded into the MSNs was greatly increased. The amount of GC within the MSNs and particle size could be controlled by adjusting the content of GA solution in the reaction system. Furthermore, this improved method ensures good spherical structure and dispersion of Gd-MSNs, simplifies the experimental steps and increases reproducibility.

In previous studies, Gd chloride and Gd oxide were most widely used in the synthesis of Gd-MSNs [35, 36]. As a simple compound, the Gd ions contained therein leached easily, causing toxicity [37]. Other studies used stable Gd chelates with safe performance, such as Gd-DTPA and Gd-DOTA [38-40]. Gd chelates have a large molecular weight and are more difficult to dope into the nanopores of MSNs than small-molecular-weight particles. The molecu-

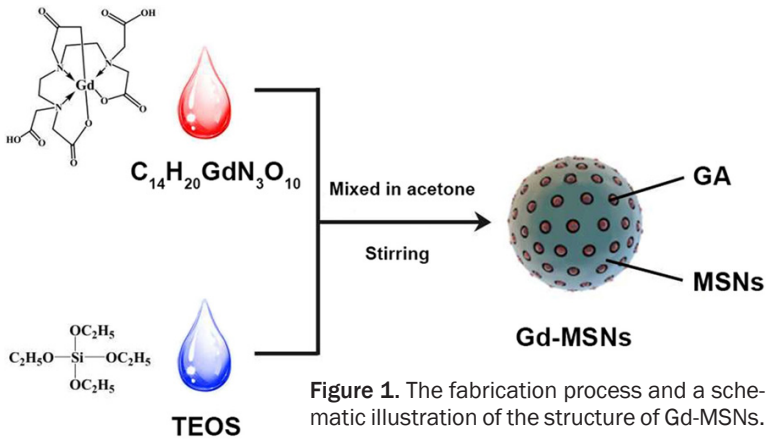

Figure 1. The fabrication process and a schematic illustration of the structure of Gd-MSNs.

lar weight of Gd-DTPA is approximately 938, and Gd-DOTA is approximately 580. Thus, a relatively small-molecular-weight Gd chelate is needed. We innovatively utilized GA (molecular weight of approximately 547), an important intermediate during the synthesis of Gd-DTPA, as the imaging agent to synthesize a new type of Gd-MSNs.

In this study, we first employed a simple and easy reverse microemulsion method using GA as an MRI contrast agent to synthesize a new type of Gd-MSN; a schematic diagram is shown in **Figure 1**. Adding GA in this method to obtain Gd-MSNs in a single step greatly simplified the process and greatly increased its reproducibility. We expect to synthesize a novel, multifunctional and highly efficient MRI contrast agent that has a relatively high GC, uniform and controllable particle size distribution, and excellent enhanced imaging capabilities *in vitro* and *in vivo*.

Materials and methods

Materials

Triton X-100, cyclohexane and 1-hexanol were purchased from Alfa Aesar Co. (Ward Hill, MA, USA). TEOS, GA, Cell Counting Kit-8 (CCK-8) and fetal bovine serum (FBS) were purchased from Sigma Aldrich Co. (St. Louis, MO, USA). Acetone, anhydrous ethanol, and ammonia solution (25-28%) were purchased from Chuandong Chemical Co, Ltd. (Chongqing, China). A dialysis bag with a 1000-Da cutoff was obtained from Spectrum Labs (Torrance, CA, USA). All chemicals were reagent grade and were used as supplied.

Synthesis of Gd-MSNs

The Gd-MSNs and MSNs were synthesized by a reverse microemulsion method [41]. Gd-MSNs with different GCs were synthesized first. A mixture of Triton X-100 (1.77 mL), cyclohexane (7.5 mL) and 1-hexanol (1.8 mL) was stirred for 10 min. A GA aqueous solution at a concentration of 0.274 g/mL was prepared. Different amounts (0.5, 1, 2, 3, 4, and 5 mL) of GA aqueous solution were then separately added to the mixture. The resulting mixtures were stirred for an additional 30 min followed by the addition of TEOS (100 μL) and an additional 30 min of stirring. Ammonia solution (1.5 mL) was added, and the reaction mixture was stirred for 6 h until a microemulsion was obtained. Finally, acetone (4 mL) was added to break the emulsion. The particles were isolated by centrifugation and washing with water and ethanol. Six groups of Gd-MSNs with different GCs were obtained and named A, B, C, D, E, and F. Second, MSNs were synthesized using the same procedures, except that 2 mL of water rather than the GA aqueous solution was added, and this group was named G.

Characterization of Gd-MSNs

Five milligrams of Gd-MSNs with different GCs (groups A-F) and MSNs were dissolved in 1 mL of hydrofluoric acid and diluted to 10 mL with water. The morphologies of the Gd-MSNs and MSNs were observed by transmission electron microscopy (TEM) at 80 kV (H-7500, Hitachi, Tokyo, Japan). The diameter and zeta potential of the Gd-MSNs and MSNs were estimated with a Malvern Zetasizer Nano ZS90 (Malvern Instrument, UK). The GCs in the NPs were determined using an inductively coupled plasma-atomic emission spectrometer (ICP-AES) (ICAP 6300 Duo, Thermo Fisher, USA). The data were collected in triplicate.

Gd-MSNs (group C, which had the highest GC, was chosen) were dispersed in PBS (5 mg/L) and added to a dialysis tube (1,000 kD), which was then soaked in 100 mL of PBS. The reaction system was placed into a 37°C incubator shaker, and the GCs were detected three times

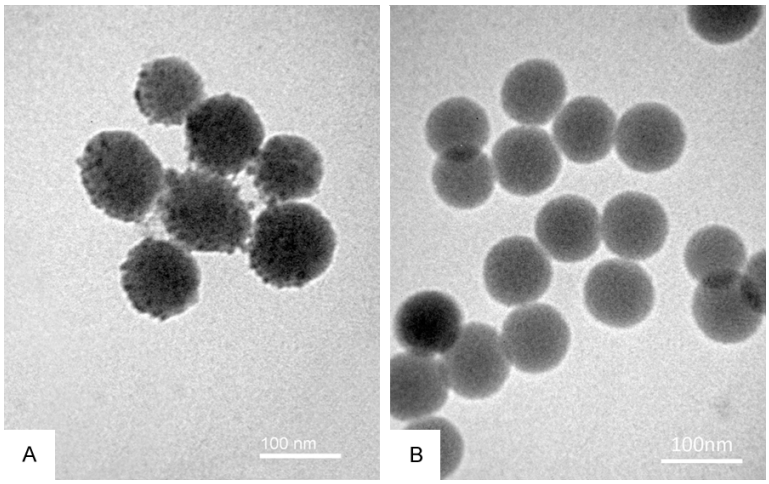

Figure 2. TEM images of Gd-MSNs (A) and MSNs (B).

Table 1. The effect of gadopentetic acid (GA) dosing on NP characteristics

Group	Batch: input of GA (mL)	Size (mean ± SD) (d, nm)	Zeta Potential (mV)	PDI	GCs (mean ± SD) (μg/mL)
A	0.5	105.7 ± 50.52	-33.9 ± 4.82	0.132	10.77 ± 0.10
B	1	115.3 ± 59.33	-37.8 ± 4.18	0.180	32.56 ± 0.32
C	2	128.6 ± 61.50	-40.9 ± 4.98	0.145	60.53 ± 0.53
D	3	121.8 ± 48.97	-39.4 ± 4.33	0.128	34.96 ± 0.28
E	4	116.1 ± 62.44	-43.2 ± 5.00	0.174	27.18 ± 0.45
F	5	109.6 ± 62.74	-32.6 ± 4.37	0.139	19.32 ± 0.16
G	0	130.7 ± 71.80	-41.5 ± 5.76	0.196	0.00 ± 0.00

by ICP-AES after shaking for 12, 24, 48, 72, and 96 h to evaluate the stability of the Gd-MSNs.

Cell viability test of Gd-MSNs

The human prostate adenocarcinoma cell line (PC-3) was purchased from Procell Life Science and Technology Co., LTD (Wuhan, China). The cells were cultured in Hams F-12 medium (Corning, USA) with 10% FBS and 1% penicillin/streptomycin (Sigma Aldrich Co., St. Louis, MO, USA). The human umbilical vein endothelial cell (HUVEC) line was obtained from the Institute of Ultrasound Imaging of Chongqing Medical University and cultured in RPMI 1640 and Dulbecco's modified Eagle medium (DMEM) (Corning, USA) with 10% FBS and 1% penicillin/streptomycin.

To test the cell viability with the CCK-8 assay, the PC-3 cell line (1×10^4 cells per well) and HUVEC cell line (1×10^4 cells per well) were incubated with various amounts (25, 50, 100, 200, and 400 μg/mL) of Gd-MSNs (group C, which had the highest GC, was chosen) in a 96-well microplate for 24 h; untreated cells served as the control. Each concentration was tested five times. The cells were washed twice with PBS; then, the CCK8 solution (10 μL) was added to each well. After 4 h, the absorbance was measured using a Bio-Tek absorbance microplate reader (ELx 800, Bio-Tek Instruments Inc., Winooski, VT, USA) at 450 nm.

In vitro MRI of Gd-MSNs

According to the ICP test results, we chose groups B, C and D, which had relatively higher GCs, for *in vitro* MR imaging. The Gd-MSNs and MSNs were dispersed in water (5 mg/mL). The four tubes were subjected to MRI scanning. Second, different concentrations of Gd-MSNs (1.6, 3.2, 6.4 and 12.8 mg/mL) (group C, which had the highest GC) were dispersed in water, and the four tubes were then subjected to MRI scanning.

MR images were acquired on an MRI scanner (Achieva 3.0T TX, Philips Healthcare, Best, the Netherlands) using an eight-channel head coil. T_1-weighted images were acquired using a fast field echo (FFE) sequence with the following parameters: TR/TE = 190/2.24 ms; FOV = 180×34; and matrix = 420×264. T_2-weighted images were acquired using a turbo spin echo (TSE) sequence with the following parameters: TR/TE = 1249.58/100 ms; FOV = 178×34; matrix = 400×259; and axial slice thickness = 6 mm. The signal intensities (SIs) of each group of NPs and water were measured three times, and the relative SI (SIr) between the NPs and water was calculated.

In vitro MRI of RAW264.7 cells

RAW264.7 mouse mononuclear macrophage leukemia cells were obtained from the Institute

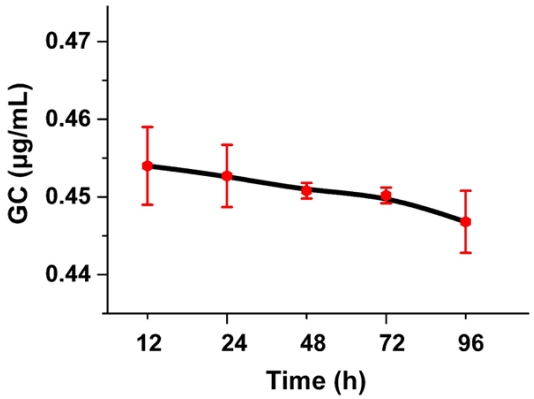

Figure 3. GC of Gd-MSN dialysates at each time point as detected by ICP-AES.

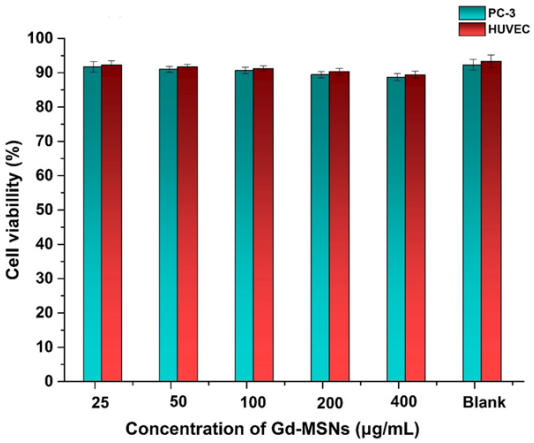

Figure 4. Cell viability of PC-3 and HUVEC cell lines incubated with different concentrations of Gd-MSNs.

of Ultrasound Imaging of Chongqing Medical University.

RAW264.7 cells were trypsinized, and an aliquot of cell suspension was added to each culture flask to obtain a cell density of 5.0×10^6 cells per flask, followed by DMEM (Corning). The flasks were then incubated (37°C, 5% CO_2) for 24 h. Next, the medium was removed and replaced with Gd-MSNs (0.6 mg and 1.8 mg) in 3 mL of media. The final Gd-MSN concentrations were 0.2 and 0.6 mg/mL. The flasks were incubated for 2 h. The cells were subsequently trypsinized, resuspended in 1 mL of DMEM, and centrifuged at 1,000 rpm for 5 min to obtain cell pellets. T_1- and T_2-weighted MR images of the pellets were obtained on an MRI scanner with the same imaging parameters as those used for the *in vitro* MRI of Gd-MSNs. RAW264.7 cells without Gd-MSNs served as the control. The SIs of RAW264.7 cells with and without Gd-MSNs were measured three times. The SIr between the cells and water was calculated.

In vivo MRI

Five male Sprague-Dawley (SD) rats that weighed between 190 and 210 g each were purchased from the Animal Center of Chongqing Medical University. The animal experiments were approved by our animal ethics committee and were conducted under protocols approved by the Institutional Animal Care and Use Committee of Chongqing Medical University. All rats were anesthetized by isoflurane inhalation anesthesia. The same MRI scanner used in the *in vitro* experiment and a rat experimental coil were used. T_1- and T_2-weighted MR images of the abdomen were acquired using a TSE sequence before and at 5, 15, 25 and 35 min after injecting Gd-MSNs at a dose of 20 mg/kg via tail vein injection. The imaging parameters for TSE T_1WI were TR/TE = 823.98/10 ms; FOV = 180×34; matrix = 420×264; flip angle = 90°; and axial slice thickness = 3 mm. The imaging parameters for TSE T_2WI were TR/TE = 2001.87/80 ms; FOV = 178×34; matrix = 400×259; flip angle = 90°; and axial slice thickness = 3 mm. Regions of interest (ROIs) were selected in the right lobe of the liver, right renal cortex, renal pelvis and psoas major muscle of each rat with an area of 2.0 mm^2 to avoid large blood vessels. Then, ROIs were selected in the aorta, hepatic vein and inferior vena cava with an area of 0.2 mm^2. The SIs of the liver, renal cortex, renal pelvis, psoas major muscle, aorta, hepatic vein and inferior vena cava were measured three times, and the SIr between the renal cortex, renal pelvis and the psoas major muscle were calculated.

Statistical analyses

The data were analyzed using the Statistical Program for Social Sciences (SPSS for Windows, version 22.00, Chicago, IL, USA). The continuous variables are presented as the means ± standard deviations, and the categorical variables are reported numerically and as percentages. Multi-group comparisons of the GC, stability and cell viability of Gd-MSNs were conducted by a one-way analysis of variance (ANOVA), and post hoc comparisons of GCs were performed by the Students-Newman-

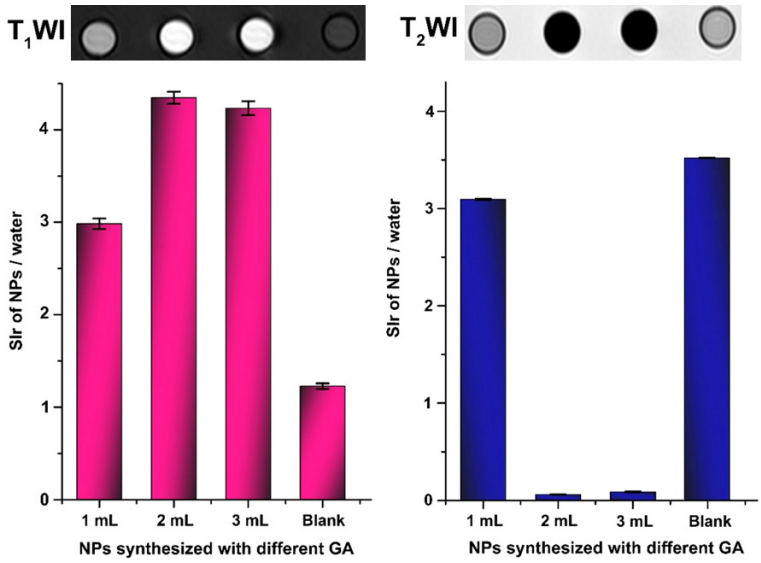

Figure 5. MRI images and T_1 and T_2 SIrs of Gd-MSNs synthesized with 1-3 mL of GA and MSNs.

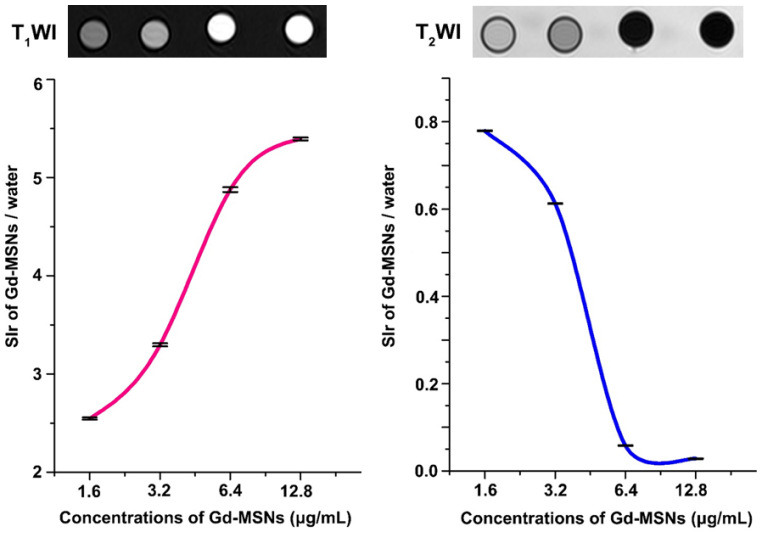

Figure 6. MR images of Gd-MSNs (group C) at different concentrations and their SIr values.

dispersed, spherically shaped NPs, and a rounded mesoporous structure with many black spots corresponding to the doped GA and a few black spots adhered to the surface of the NPs (**Figure 2A**). Black spots could not be found on the mesoporous structure of the MSNs (**Figure 2B**). The characteristics of the NPs are summarized in **Table 1**. One-way ANOVA of the diameters among the groups of NPs showed no significant differences (F = 1.192, P = 0.310). There were significant GC differences among the groups of Gd-MSNs (F = 7476.673, P = 0.000). The Students-Newman-Keuls test was used for inter-group comparisons, and significant differences were found between any two groups (P < 0.05). The maximum GC was 60.53 ± 0.53 μg/mL when 2 mL of GA solution was added (group C).

The GCs in the dialysate were detected by ICP-AES and are presented in **Figure 3**. One-way ANOVA of the GCs of Gd-MSNs showed no significant differences at the 5 time points analyzed between 12 h and 96 h (F = 2.059, P = 0.162), indicating that the chemical construction of the Gd-MSNs was very stable in a simulated *in vitro* environment.

Keuls test. Post hoc comparisons of stability and cell viability were conducted using the Bonferroni test. Statistical significance was defined as P < 0.05.

Results

Characterization of Gd-MSNs

Gd-MSNs and MSNs were successfully synthesized with the reverse microemulsion method. All types of NPs were obtained as white powders. TEM images of Gd-MSNs showed mono-

Cell viability test

The cell viability of PC-3 and HUVECs incubated with Gd-MSNs for 24 h at different concentrations (25, 50, 100, 200 and 400 μg/mL) are compared in **Figure 4**. One-way ANOVA of PC-3 and HUVECs showed a significant difference (F_{pc3} = 6.742, P_{pc3} = 0.000; F_{HUVEC} = 7.557, P_{HUVEC} = 0.000). The Bonferroni test was performed for inter-group comparisons. Significant differences were not found between the 25, 50, and 100 μg/mL and control groups (P > 0.05). Thus,

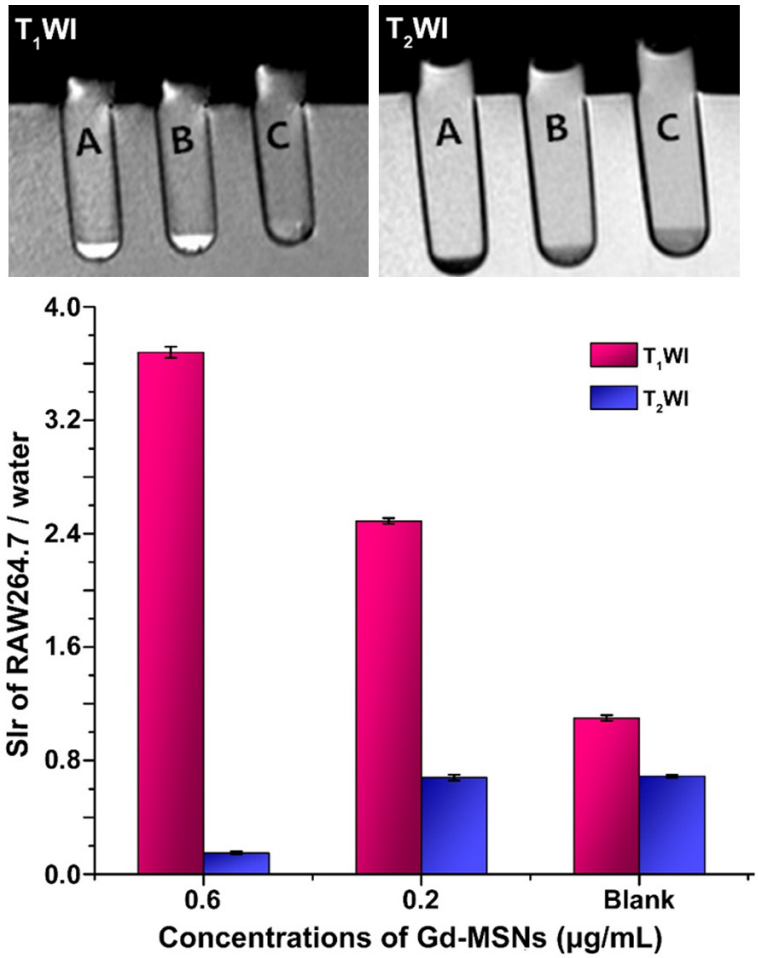

Figure 7. T_1-weighted (left) and T_2-weighted (right) MR images of RAW264.7 cells incubated with Gd-MSNs and their SIr values.

cell viability was not affected in this concentration range. Significant differences were found between the 200 μg/mL and control groups (P_{pc3} = 0.011, P_{HUVEC} = 0.005), the 400 μg/mL and control groups (P_{pc3} = 0.001, P_{HUVEC} = 0.000), and the 400 μg/mL and 25 μg/mL groups (P_{pc3} = 0.007, P_{HUVEC} = 0.008), indicating that cell viability decreased at the 200 μg/mL and 400 μg/mL concentrations.

In vitro MRI of Gd-MSNs

The MR images and their SIr values of T_1- and T_2-weighted MR images of Gd-MSNs (groups B, C and D) and MSNs are presented in **Figure 5**. Compared with water, all NPs were enhanced on the T_1-weighted images and decreased on the T_2-weighted images. In particular, significant T_1-weighted enhancement and T_2-weighted signal loss were clearly observed in the three groups of Gd-MSNs compared to the MSNs (F_{T1} = 1745.535, P_{T1} = 0.000; F_{T2} = 2687411.123, P_{T2} = 0.000). The maximum and minimum SIr of Gd-MSNs on the T_1- and T_2-weighted images were 4.35 ± 0.07 and 0.01 ± 0.00, respectively, in group C.

The MR images and their SIr values of T_1- and T_2-weighted MR images of Gd-MSNs at different concentrations are provided in **Figure 6**. The signals increased on the T_1-weighted images and decreased on the T_2-weighted images as the concentrations increased.

In vitro MRI of RAW264.7 cells

T_1- and T_2-weighted MR images of RAW264.7 cells incubated with 0.2 and 0.6 mg/mL Gd-MSNs for 2 h are shown in **Figure 7**. Significant T_1-weighted enhancement and T_2-weighted signal loss were clearly observed in the two groups of cells containing Gd-MSNs compared with the control group.

In vivo MRI

T_1- and T_2-weighted MR images were successfully obtained pre-contrast and then at 5, 15, 25, and 35 min after injecting Gd-MSNs at a dose of 20 mg/kg via the tail vein. The liver, aorta, hepatic vein, and inferior vena cava were significantly enhanced on T_1WI, and T_1-weighted enhancement was clearly observed in the renal cortex and renal pelvis. Significant T_2-weighted signal loss was clearly observed in the liver and renal cortex (**Figure 8**).

T_1-weighted MR images of the kidneys obtained pre-contrast and 5, 15, 25 and 35 min after the injection of Gd-MSNs at a dose of 20 mg/kg via the tail vein are shown in **Figure 9**. The SI values of the renal cortex, renal pelvis, and the psoas major muscle were measured, and the SIr values of the renal cortex, renal pelvis and psoas major muscle are shown in **Figure 9**. Five minutes after Gd-MSN injection, the renal parenchymal signal was significantly increased, and the signal from the renal cortex was signifi-

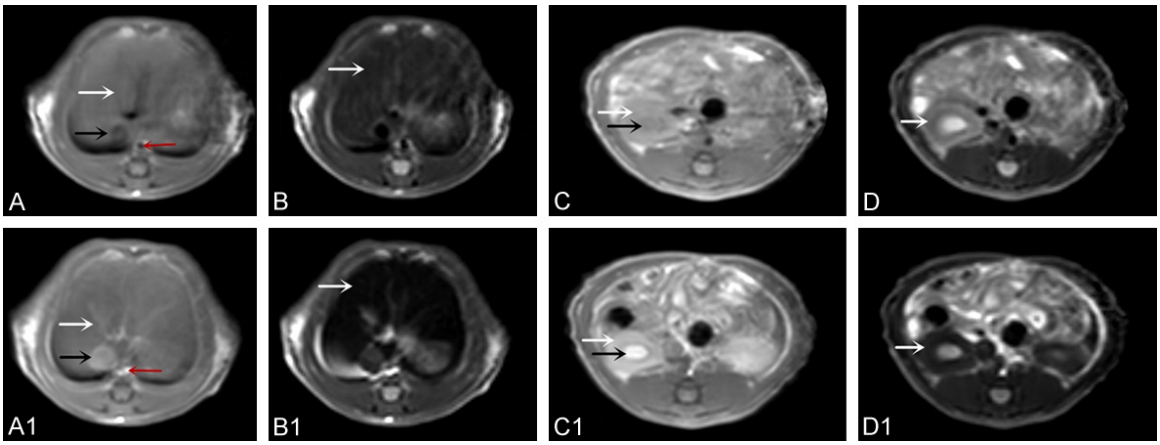

Figure 8. Rat MRI results. The white arrows in (A) (T_1 pre-contrast) and (A1) (T_1 post-contrast) indicate the hepatic vein; the black arrow indicates the inferior vena cava; and the red arrow indicates the aorta. The white arrows in (B) (T_2 pre-contrast) and (B1) (T_2 post-contrast) indicate the liver parenchyma. The white and black arrows in (C) (T_1 pre-contrast) and (C1) (T_1 post-contrast) indicate the renal cortex and renal pelvis, respectively. The white arrows in (D) (T_2 pre-contrast) and (D1) (T_2 post-contrast) indicate the renal cortex.

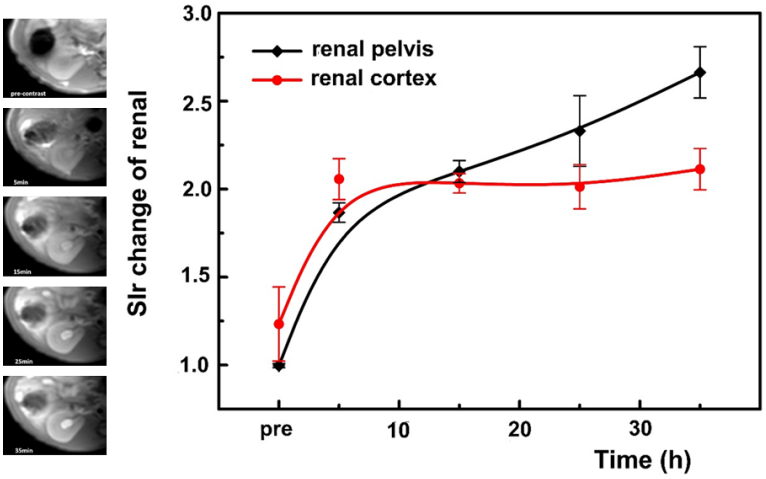

Figure 9. T_1-weighted rat kidney MR images and the SIr values of the kidney at different time points.

cantly higher than that of the renal pelvis. Subsequently, in scans at 15, 25, and 35 min, the renal cortical signal decreased gradually, whereas the renal pelvis signal increased gradually. At 25 min after Gd-MSN injection, the renal pelvis signal was significantly higher than in the renal cortex.

Discussion

Gd-MSNs and MSNs were successfully synthesized in this study. TEM images revealed a clearly visible pore structure with a large number of doped GA molecules on the Gd-MSNs prepared in this study. The results of ICP-AES showed that the GCs of the Gd-MSNs were obviously higher than those of the Gd chelate-doped MSNs reported in the literature [20, 24, 30]. GA has a lower molecular weight than Gd chelates because GA does not contain a meglumine group. Thus, GA is more easily doped into the nanopores of MSNs, which can greatly increase both the carrying capacity of Gd and the capability of Gd-MSNs to exhibit shortened relaxation times. The ICP-AES results also showed that the GCs of Gd-MSNs increased as the amount of GA solution increased; the maximum GC was 60.53 ± 0.53 μg/mL when 2 mL of GA solution was added. In contrast, when more than 2 mL of GA was added, the GCs gradually decreased. In the *in vitro* experiment, the Gd-MSNs exhibited good stability in a simulated *in vitro* environment. In the cell viability test, the Gd-MSNs exerted no obvious toxicity in the cells over a certain concentration range, indicating that the Gd-MSNs are a very effective, safe and stable MR contrast agent.

The *in vitro* MR images showed that the Gd-MSNs could increase the SIr on T_1WI and decrease the SIr on T_2WI better than MSNs. The NP properties that shorten the relaxation

time are mainly the result of the Gd^{3+} ions doped into the mesoporous particles, which results in para-magnetism [42]. As the GC increased, the paramagnetic properties improved; the ability of the NPs to shorten the relaxation time increased; the SIr on T_1WI increased; and the SIr on T_2WI decreased. RAW264.7 cell phantom MR images showed that the relaxation time of the cells incubated with Gd-MSNs was significantly shortened, and the signal was enhanced on T_1WI and decreased on T_2WI relative to the cells without Gd-MSNs. Additionally, as the concentration of Gd-MSNs increased, the enhancement effect became more obvious. These integrated T_1- and T_2-weighted MR modalities could potentially offer more complete and accurate information about lesions by overcoming the shortcomings of each single MR mode.

Based on the above results, we speculate that the GC of Gd-MSNs may be affected by the following two factors. The first factor is the GA content in the microemulsion system. Within a certain range, the GA doped into the mesopores of Gd-MSNs increased until the mesopores were all occupied by GA. Subsequently, the GC of the Gd-MSNs did not continue to increase, even if additional GA was added. At this point, the GCs of the NPs depended mainly on the amount of GA in the microemulsion system. Thus, the GCs in groups A-C gradually increased until saturation was reached after the addition of 2 mL of GA solution. Beyond this point, the GCs did not increase further. The second factor was the water content in the microemulsion system. Previous research has revealed that the water content in the microemulsion system exerts an important impact on the particle size of the MSNs [43, 44]. The TEOS cannot be completely hydrolyzed if the water content is too low. In contrast, when the water content is too high, the water generated during the condensation process will negatively impact the concentration of the hydrolysis product. Therefore, when too little or too much water was present, the MSNs had small particle sizes. Using the correct amount of water ensures both the complete hydrolysis of TEOS and high concentrations of hydrolysate, resulting in MSNs with large particle sizes, homogeneous compositions and good dispersions. In our experiment, after GA saturation, the GCs of the Gd-MSNs mainly depended on the diameters of the NPs themselves. As the amount of GA solution increased, the amount of water in the reaction system also increased. Thus, the particle size of the resulting Gd-MSNs decreased gradually, and the GCs of the individual NPs also decreased. Therefore, the GCs of the Gd-MSNs in groups D-F decreased as the GA solution added increased.

In vivo MR images showed that the SI values of the aorta, hepatic vein and inferior vena cava were significantly enhanced on T_1WI. Moreover, the liver parenchyma, renal cortex and renal pelvis were increased on T_1WI and decreased on T_2WI after the injection of a low concentration of Gd-MSNs in SD rats, which confirmed the presence of good relaxation properties *in vivo*. Regarding the enhanced MRI results of the kidneys on T_1WI, the renal pelvis and cortex showed significant enhancement compared with the pre-contrast image. Five min after Gd-MSN injection, the renal cortex and medullary regions were clearly demarcated, and the renal cortical signal was the highest. Thus, at 5 min post-injection, the Gd-MSNs had reached the renal parenchyma. Subsequently, the signal in the renal cortex remained constant as the excretion of Gd-MSN plateaued. After 15 min, the renal cortical signal gradually decreased, possibly because of the gradual excretion of Gd-MSNs to the renal pelvis. The signal in the renal pelvis continuously increased because of the continuous excretion of Gd-MSNs by the kidneys. As a result, the concentration in the renal pelvis increased. The preliminary animal experiments revealed that, in vivo, a relatively low concentration of Gd-MSNs could significantly shorten the relaxation time of tissue on T_1WI and T_2WI and thereby achieve enhancement. Gd-MSNs are mainly metabolized by the liver and are gradually excreted by the kidneys after being injected into the blood circulation. Gd-MSNs have a longer blood circulation time, which is highly advantageous for the further preparation of targeted nano-contrast agents. Small doses of these NPs can achieve enhancing effect, and the small particle size increases the cycle time in the blood circulation, which greatly reduces the required dose of contrast agent and the incidental side effects [45].

This study had some limitations. The Malvern Zetasizer test results indicated that the NP particle size was right-skewed, and a small number of large NPs existed (indicating minimal aggregation of NPs). We will further improve the syn-

thesis method to make the dispersity of the Gd-MSNs better. The use of GA in this study led to higher GCs. We will optimize the solution in future applications. Animal experiments are preliminary, and the *in vivo* metabolism and toxicity of Gd-MSNs were not studied in this work. These issues will be studied in future projects.

Through *in vitro* and *in vivo* studies, we have confirmed that Gd-MSNs make an excellent MR nano-contrast agent. Gd-MSNs are easy to modify and have the potential to connect various functional groups. Gd-MSNs can be used for molecular targeted imaging by connecting with targeted groups and can facilitate multimodal imaging when combined with microbubble or fluorescent imaging agents. Targeted Gd-MSNs can carry a variety of chemotherapy drugs to achieve targeted tumor therapy, the mesoporous channels of Gd-MSNs can also be modified to facilitate controlled drug-specific release in an organized manner. These topics are the focus of our future experiments.

Conclusions

In this study, we designed and characterized novel Gd-MSNs with high GCs and extraordinary abilities to enhance MR images. These NPs were stable and safe under normal physiological conditions. Their utility as a contrast agent for MRI was clearly demonstrated both *in vitro* and *in vivo*. Gd-MSNs have great potential for targeted applications and are expected to become a novel, multifunctional and highly efficient MRI contrast agent because of their easy modification.

Acknowledgements

We acknowledge financial support from the National Natural Science Foundation of China (81401382). We thank Professor Ying Zhuo from Southwest University for suggesting the experiment. We are grateful to American Journal Experts (AJE) for their assistance with language editing.

Disclosure of conflict of interest

None.

Abbreviations

MSNs, mesoporous silica nanoparticles; GA, gadopentetic acid; Gd-MSNs, gadolinium-doped mesoporous silica nanoparticles; GC, gadolinium content; ICP-AES, inductively coupled plasma-atomic emission spectroscopy; TEM, transmission electron microscopy; MRI, magnetic resonance imaging; NPs, nanoparticles; SEM, scanning electron microscopy.

Address correspondence to: Dr. Xiaojing He, Department of Radiology, The Second Affiliated Hospital of Chongqing Medical University, No. 74 Linjiang Rd, Yuzhong District, Chongqing 400010, China. Tel: +86 23 63693238; E-mail: He_xiaojing1006@163.com

References

[1] Caravan P, Ellison JJ, McMurry TJ and Lauffer RB. Gadolinium (III) chelates as MRI contrast agents: structure, dynamics, and applications. Chem Rev 1999; 99: 2293-2352.

[2] Adusumilli S and Pretorius ES. Magnetic resonance imaging of prostate cancer. Semin Urol Oncol 2002; 20: 192-210.

[3] Deroose CM, De A, Loening AM, Chow PL, Ray P, Chatziioannou AF and Gambhir SS. Multimodality imaging of tumor xenografts and metastases in mice with combined small-animal PET, small-animal CT, and bioluminescence imaging. J Nucl Med 2007; 48: 295-303.

[4] Ananta JS, Godin B, Sethi R, Moriggi L, Liu X, Serda RE, Krishnamurthy R, Muthupillai R, Bolskar RD, Helm L, Ferrari M, Wilson LJ and Decuzzi P. Geometrical confinement of gadolinium-based contrast agents in nanoporous particles enhances T1 contrast. Nat Nanotechnol 2010; 5: 815-821.

[5] Choi KY, Liu G, Lee S and Chen X. Theranostic nanoplatforms for simultaneous cancer imaging and therapy: current approaches and future perspectives. Nanoscale 2012; 4: 330-342.

[6] Gizzatov A, Hernández-Rivera M, Keshishian V, Mackeyev Y, Law JJ, Guven A, Sethi R, Qu F, Muthupillai R, Cabreira-Hansen Mda G, Willerson JT, Perin EC, Ma Q, Bryant RG and Wilson LJ. Surfactant-free Gd(3+)-ion-containing carbon nanotube MRI contrast agents for stem cell labeling. Nanoscale 2015; 7: 12085-12091.

[7] Zhang LX, Li KF, Wang H. Preparation and in vitro evaluation of a MRI contrast agent based on aptamer-modified gadolinium-loaded liposomes for tumor targeting. AAPS PharmSciTech 2017; 18: 1564-1571.

[8] Zhao L, Zheng Y, Yan H, Xie W, Sun X, Li N and Tang J. 2-deoxy-D-glucose modified magnetic nanoparticles with dual functional properties: nanothermotherapy and magnetic resonance imaging. J Nanosci Nanotechnol 2016; 16: 2401-2407.

[9] Hou L, Yang X, Ren J, Wang Y, Zhang H, Feng Q, Shi Y, Shan X, Yuan Y and Zhang Z. A novel redox-sensitive system based on single-walled carbon nanotubes for chemo-photothermal therapy and magnetic resonance imaging. Int J Nanomed 2016; 11: 607-624.
[10] Lin W, Hyeon T, Lanza GM, Zhang M and Meade TJ. Magnetic nanoparticles for early detection of cancer by magnetic resonance imaging. MRS Bull 2009; 34: 441-448.
[11] Seeta Rama Raju G, Benton L, Pavitra E and Yu JS. Multifunctional nanoparticles: recent progress in cancer therapeutics. Chem Commun 2015; 51: 13248-13259.
[12] Estelrich J, Sánchez-Martín MJ and Busquets MA. Nanoparticles in magnetic resonance imaging: from simple to dual contrast agents. Int J Nanomed 2015; 10: 1727-1741.
[13] Hashim Z, Green M, Chung PH, Suhling K, Protti A, Phinikaridou A, Botnar R, Khanbeigi RA, Thanou M, Dailey LA, Commander NJ, Rowland C, Scott J and Jenner D. Gd-containing conjugated polymer nanoparticles: bimodal nanoparticles for fluorescence and MRI imaging. Nanoscale 2014; 6: 8376-8386.
[14] Luchini A, Heenan RK, Paduano L and Vitiello G. Functionalized SPIONs: the surfactant nature modulates the self-assembly and cluster formation. Phys Chem Chem Phys 2016; 18: 18441-18449.
[15] Zhao H, Chao Y, Liu J, Huang J, Pan J, Guo W, Wu J, Sheng M, Yang K, Wang J and Liu Z. Polydopamine coated single-walled carbon nanotubes as a versatile platform with radionuclide labeling for multimodal tumor imaging and therapy. Theranostics 2016; 6: 1833-1843.
[16] Torchilin VP. Liposomes as delivery agents for medical imaging. Mol Med Today 1996; 2: 242-249.
[17] Liberman A, Mendez N, Trogler WC and Kummel AC. Synthesis and surface functionalization of silica nanoparticles for nanomedicine. Surf Sci Rep 2014; 69: 132-158.
[18] Douroumis D, Onyesom I, Maniruzzaman M and Mitchell J. Mesoporous silica nanoparticles in nanotechnology. Crit Rev Biotechnol 2013; 33: 229-245.
[19] Qiao B, Liang Y, Wang TJ and Jiang Y. Surface modification to produce hydrophobic nano-silica particles using sodium dodecyl sulfate as a modifier. Appl Surf Sci 2016; 364: 103-109.
[20] Taylor KM, Kim JS, Rieter WJ, An H, Lin W and Lin W. Mesoporous silica nanospheres as highly efficient MRI contrast agents. J Am Chem Soc 2008; 130: 2154-2155.
[21] Mehravi B, Ardestani MS, Damercheli M, Soltanghoraee H, Ghanaldarlaki N, Alizadeh AM, Oghabian MA, Shirazi MS, Mahernia S and Amanlou M. Breast cancer cells imaging by targeting methionine transporters with gadolinium-based nanoprobe. Mol Imaging Biol 2014; 16: 519-528.
[22] Kim J, Kim HS, Lee N, Kim T, Kim H, Yu T, Song IC, Moon WK and Hyeon T. Multifunctional uniform nanoparticles composed of a magnetite nanocrystal core and a mesoporous silica shell for magnetic resonance and fluorescence imaging and for drug delivery. Angew Chem Int Ed 2008; 47: 8438-8441.
[23] Kim T, Momin E, Choi J, Yuan K, Zaidi H, Kim J, Park M, Lee N, McMahon MT, Quinones-Hinojosa A, Bulte JW, Hyeon T and Gilad AA. Mesoporous silica-coated hollow manganese oxide nanoparticles as positive T1 contrast agents for labeling and MRI tracking of adipose-derived mesenchymal stem cells. J Am Chem Soc 2011; 133: 2955-2961.
[24] Hsiao JK, Tsai CP, Chung TH, Hung Y, Yao M, Liu HM, Mou CY, Yang CS, Chen YC and Huang DM. Mesoporous silica nanoparticles as a delivery system of gadolinium for effective human stem cell tracking. Small 2008; 4: 1445-1452.
[25] Shao Y, Tian X, Hu W, Zhang Y, Liu H, He H, Shen Y, Xie F and Li L. The properties of Gd2-O3-assembled silica nanocomposite targeted nanoprobes and their application in MRI. Biomaterials 2012; 33: 6438-6446.
[26] Stöber W, Fink A and Bohn E. Controlled growth of monodisperse silica spheres in the micron size range. J Colloid Interface Sci 1968; 26: 62-69.
[27] Mehravi B, Ahmadi M, Amanlou M, Mostaar A, Ardestani MS and Ghalandarlaki N. Cellular uptake and imaging studies of glycosylated silica nanoprobe (GSN) in human colon adenocarcinoma (HT 29 cell line). Int J Nanomed 2013; 8: 3209-3216.
[28] Mehravi B, Ahmadi M, Amanlou M, Mostaar A, Ardestani MS and Ghalandarlaki N. Conjugation of glucosamine with Gd3+-based nanoporous silica using a heterobifunctional ANB-NOS crosslinker for imaging of cancer cells. Int J Nanomed 2013; 8: 3383-3394.
[29] Li J, You J, Dai Y, Shi M, Han C and Xu K. Gadolinium oxide nanoparticles and aptamer-functionalized silver nanoclusters-based multimodal molecular imaging nanoprobe for optical/magnetic resonance cancer cell imaging. Anal Chem 2014; 86: 11306-11311.
[30] Carniato F, Tei L, Arrais A, Marchese L and Botta M. Selective anchoring of Gd (III) chelates on the external surface of organo-modified mesoporous silica nanoparticles: a new chemical strategy to enhance relaxivity. Chemistry 2013; 19: 1421-1428.
[31] Nandiyanto ABD, Kim SG, Iskandar F and Okuyama K. Synthesis of spherical mesopo-

rous silica nanoparticles with nanometer-size controllable pores and outer diameters. Micropor Mesopor Mater 2009; 120: 447-453.
[32] Auger A, Samuel J, Poncelet O and Raccurt O. A comparative study of non-covalent encapsulation methods for organic dyes into silica nanoparticles. Nanoscale Res Lett 2011; 6: 328.
[33] Yamauchi H, Ishikawa T and Kondo S. Surface characterization of ultramicro spherical particles of silica prepared by w/o microemulsion method. Colloids Surf 1989; 37: 71-80.
[34] Bagwe RP, Yang C, Hilliard LR and Tan W. Optimization of dye-doped silica nanoparticles prepared using a reverse microemulsion method. Langmuir 2004; 20: 8336-8342.
[35] Shen Y, Shao Y, He H, Tan Y, Tian X, Xie F, Li L. Gadolinium(3+)-doped mesoporous silica nanoparticles as a potential magnetic resonance tracer for monitoring the migration of stem cells in vivo. Int J Nanomed 2013; 8: 119-127.
[36] Gupta N, Shrivastava A and Sharma RK. Silica nanoparticles coencapsulating gadolinium oxide and horseradish peroxidase for imaging and therapeutic applications. Int J Nanomed 2012; 7: 5491-5500.
[37] Zhang S, Jiang Z, Liu X, Zhou L and Peng W. Possible gadolinium ions leaching and MR sensitivity over-estimation in mesoporous silica-coated upconversion nanocrystals. Nanoscale 2013; 5: 8146-8155.
[38] Gizzatov A, Stigliano C, Ananta JS, Sethi R, Xu R, Guven A, Ramirez M, Shen H, Sood A, Ferrari M, Wilson LJ, Liu X and Decuzzi P. Geometrical confinement of Gd (DOTA) molecules within mesoporous silicon nanoconstructs for MR imaging of cancer. Cancer Lett 2014; 352: 97-101.
[39] Hu H, Arena F, Gianolio E, Boffa C, Di Gregorio E, Stefania R, Orio L, Baroni S and Aime S. Mesoporous silica nanoparticles functionalized with fluorescent and MRI reporters for the visualization of murine tumors overexpressing αvβ3 receptors. Nanoscale 2016; 8: 7094-7104.
[40] Taylor-Pashow KM, Della Rocca J and Lin W. Mesoporous silica nanoparticles with Co-condensed gadolinium chelates for multimodal imaging. Nanomaterials (Basel) 2012; 2: 1-14.
[41] Arriagada FJ and Osseo-Asare K. Synthesis of nanosize silica in a nonionic water-in-oil microemulsion: effects of the water/surfactant molar ratio and ammonia concentration. J Colloid Interface Sci 1999; 211: 210-220.
[42] Lauffer RB. Paramagnetic metal complexes as water proton relaxation agents for NMR imaging: theory and design. Chem Rev 1987; 87: 901-927.
[43] Yao L, Xu G, Dou W and Bai Y. The control of size and morphology of nanosized silica in Triton X-100 based reverse micelle. Colloids SurfA Physicochem Eng Asp 2008; 316: 8-14.
[44] Aubert T, Grasset F, Mornet S, Duguet E, Cador O, Cordier S, Molard Y, Demange V, Mortier M and Haneda H. Functional silica nanoparticles synthesized by water-in-oil microemulsion processes. J Colloid Interface Sci 2010; 341: 201-208.
[45] Petros RA and DeSimone JM. Strategies in the design of nanoparticles for therapeutic applications. Nat Rev Drug Discov 2010; 9: 615-627.